



HAL
open science

6.6W/mm 200nm CMOS compatible AlN/GaN/Si MIS-HEMT with in-situ SiN gate dielectric and low temperature ohmic contacts

Erwan Morvan, Yveline Gobil, Fanny Morisot, Jérôme Biscarrat, Matthew Charles, Jose Lugo, Alexis Divay, Mohammed Medbouhi, Ismael Charlet, Julien Delprato, et al.

► To cite this version:

Erwan Morvan, Yveline Gobil, Fanny Morisot, Jérôme Biscarrat, Matthew Charles, et al.. 6.6W/mm 200nm CMOS compatible AlN/GaN/Si MIS-HEMT with in-situ SiN gate dielectric and low temperature ohmic contacts. IEDM 2023 - IEEE International Electron Devices Meeting, Dec 2023, San Francisco, United States. <10.1109/IEDM45741.2023.10413676>. <cea-04539880>

HAL Id: cea-04539880

<https://cea.hal.science/cea-04539880v1>

Submitted on 9 Apr 2024

HAL is a multi-disciplinary open access archive for the deposit and dissemination of scientific research documents, whether they are published or not. The documents may come from teaching and research institutions in France or abroad, or from public or private research centers.

L'archive ouverte pluridisciplinaire HAL, est destinée au dépôt et à la diffusion de documents scientifiques de niveau recherche, publiés ou non, émanant des établissements d'enseignement et de recherche français ou étrangers, des laboratoires publics ou privés.



HAL Authorization

6.6W/mm 200mm CMOS compatible AlN/GaN/Si MIS-HEMT with in-situ SiN gate dielectric and low temperature ohmic contacts

E.Morvan, Y.Gobil, F.Morisot, J.Biscarat, M.Charles, J. Lugo, A.Divay, M.Medbouhi, I.Charlet, J.Delprato, P.Scheiblin, B.Rrustemi, A.Giry, A.Serhan, S.Ruel, P.Pimenta-Barros, F.Laulagnet, S.Minoret, A.Anotta, T.Billon, B.Duriez
CEA Leti, Université Grenoble Alpes, 38000 Grenoble, France, email: erwan.morvan@cea.fr

Abstract—We report on the development of CMOS compatible SiN/AlN/GaN MIS-HEMT process on 200mm Si substrates for Ka-band power amplification. The combination of soft gate process, gate design with reduced electric field, in-situ SiN gate dielectric, low temperature ohmic contacts, low substrate RF losses and GaN:C back-barrier leads to F_t/F_{MAX} of 81/173GHz for $2 \times 50 \mu\text{m}$ devices with $L_G=150\text{nm}$. At 28 GHz, the device shows performance similar to other GaN/Si technologies at $V_{DD}=10\text{V}$ and competitive performance with GaN/SiC at $V_{DD}=20\text{V}$ with PAE=41% and $P_{SAT}=6.6\text{W/mm}$.

I. INTRODUCTION

GaN-based high electron mobility transistors (HEMT) have shown superior performance for RF applications such as mobile communication, radar, satcom, earth observation or industrial heating, due to its high breakdown field and high carrier density (N_s) and electron saturation velocity of its two dimensional electron gas (2DEG) [1]. One of the emerging mm-wave III-N HEMT technology is using ultra-thin, ultra-wide bandgap (UWBG) barrier layer, like AlN or ScAlN, to simultaneously support operation at high current, high voltage and high frequency [2],[6],[12],[14]. In order to avoid excessive gate leakage associated with ultra-thin barriers, MIS-HEMT structures have been proposed. Recently, very high performance MIS-HEMT has been demonstrated, using CMOS compatible, deeply scaled ex-situ high-k gate insulator [4],[9]. An alternative approach is to use in-situ MOCVD SiN for the gate dielectric. In-situ SiN/AlN/GaN HEMT stack has the combined advantage of high N_s with a very thin barrier layer due to the high spontaneous and piezoelectric polarization of AlN on GaN with high quality in-situ SiN layer. This structure shows very good performance up to mm-wave. However the majority of published studies are based on GaN/SiC and/or non CMOS compatible processing [5],[6],[7],[14].

In this work, we demonstrate state of the art 200mm CMOS compatible SiN/AlN/GaN/Si MIS-HEMT with in-situ SiN gate dielectric, a low damage gate process and low temperature ohmic contacts to preserve heterojunction performance. These devices are designed with a reference gate length, $L_G=150\text{nm}$ for power amplification in Ka-band.

II. DEVICE TECHNOLOGY

A. Epitaxy structure and Device Processing

The starting material is 200mm MOCVD GaN epitaxy on Si-HR <111> substrate with resistivity $> 3 \text{ k}\Omega\cdot\text{cm}$ from ENKRIS Semiconductor. It consists of nucleation and stress management layers, a carbon doped GaN buffer (GaN:C), a 150nm un-intentionally doped GaN channel (appropriate for $L_G=150\text{nm}$), a 5nm AlN barrier and an in-situ 2.5 nm SiN capping layer (Fig.1). The fully CMOS compatible, gold free process flow is summarized in Fig.2. Ar was implanted for device isolation. Fully recessed Ti/Al ohmic contacts annealed at 590°C show a contact resistance, R_c of $0.4 \Omega\cdot\text{mm}$, extracted from TLM measurement and a metal sheet resistance of $0.24\Omega/\text{sq}$. This low temperature contact avoids 2DEG properties degradation observed for high temperature contact ($>800^\circ\text{C}$) even with in-situ SiN capping layer [5]. At metal 1 level, the 2DEG sheet resistance, R_s is $220 \Omega/\text{sq}$ (Van der Pauw) close to the post-epitaxy value of $200 \Omega/\text{sq}$ (Eddy current). The gate finger has a static resistance of 0.106Ω per micron gate width for $L_G=150\text{nm}$. The sheet resistance of the $1.4 \mu\text{m}$ Ti/TiN/AlCu/Ti/TiN metal 1 interconnects is $21 \text{ m}\Omega/\text{sq}$. RF losses of $0.13 \pm 0.01 \text{ dB/mm}$ are extracted at 30 GHz from Coplanar Waveguide (CPW) S-parameters measurements at the end of the HEMT process (Fig.3). The final coplanar two finger device is shown in Fig.4. The uniformity of typical device parameters is shown in Fig.5.

Device TEM cross-section is shown in Fig.6. The dielectric stack used for the gate foot fabrication allows very soft gate processing with minimal impact on the in-situ SiN gate dielectric and heterojunction underneath. Before ALCVD TiN deposition, the bottom oxide layer is wet etched, which additionally produces rounded gate edge to minimize electric field peak at the gate corner. TCAD simulations, carried out with Sentaurus Device from Synopsys (Fig.7 and Fig.8), show the reduction of the electric field peak at gate edge due to the wet etch undercut (UC). Low field channel transport properties were measured with a gated Hall bar test structure (Fig.9). High channel sheet carrier density, N_s , and mobility, μ , associated with a low channel sheet resistance, R_s are obtained, indicating low gate process impact on the 2DEG.

B. Transistor measurement

The reference HEMT has a 150nm gate length, $2 \times 50 \mu\text{m}$ width, $L_{GS} = 0.4 \mu\text{m}$ and $L_{GD} = 1.1 \mu\text{m}$. Its DC characteristics are

shown in Fig.10. At $V_{ds}=10V$, a typical HEMT shows a high maximum drain current, $I_{D_{MAX}}$ of 1.8 A/mm at $V_{gs}=+2V$, a pinch-off voltage, V_p of -2.6V (at $V_{ds}=10V$, $I_d=100\mu A/mm$), and a $G_{m_{MAX}}$ of 610 mS/mm. In off-state at $V_{gs}=-7.1V$ I_d reached 3mA/mm at $V_{DS}=24V$. This is not a gate-drain breakdown but a D-S leakage (Fig.10.d). The onset of this leakage is strongly dependent on L_G (Fig.11) due to a short channel effect (SCE) [8] as shown in Fig.12 and Fig.13. The on-state resistance, $R_{ON} = 1.3 \text{ Ohm.mm}$ for $L_G=150nm$ (Fig.11) is mainly driven by R_c (~60%) which leaves room for improvement of this device. We have reached $R_c = 0.22 \text{ +/- } 0.014 \text{ } \Omega.mm$ with recess optimization, which would translate to $R_{ON} = 0.94 \text{ } \Omega.mm$. [3] even reached $0.15 \text{ } \Omega.mm$ with a similar contact technology. The device behaves well at $150^\circ C$ with $I_{D_{MAX}}=1.5A/mm$ (Fig.14). The temperature impact on the knee voltage is low due to the weak temperature sensitivity of R_c .

Pulsed I-V measurements were carried out on the reference HEMT with a PIV AM3200 from AMCAD Engineering. A pulse width and delay of $1\mu s$ and a duty cycle of 0.1% were used. The reference bias was $V_{gsq}/V_{dsq}=0/0V$ and the stress biases were $V_{gsOFF}/0V, /10V, /15V, /20V$ with $V_{gsOFF}= -5.1 V$. A typical pulsed-IV characteristic is shown in Fig.15. Gate lag (GL) and Drain lag (DL) are extracted from maximum power load-lines (including both knee voltage and drain current degradations due to trapping). Four dies have been measured across the wafer radius. As can be observed in Table 1, the GL is very small and the mean DL is below 10% at $V_{dsq}/V_{gsq}=20V/-5.1V$ (with similar values on 4 dies), indicating a low trapping effect and good uniformity.

S-parameters were measured using $100\mu m$ pitch GSG probes and a N5227B PNA from Keysight on a semi-automatic prober from MPI. The frequency range is 100MHz to 67GHz with an IF of 100Hz. Voltage biasing was done through the intern bias-T from the VNA and DC polarizations was applied using B1500 SMU. After de-embedding, the reference HEMT yields $F_t = 81GHz$ and $F_{MAX}=173GHz$ (Fig.16). L_G and W_G impact on F_t and F_{MAX} are described in Fig.17 and Fig.18, respectively. F_t does not increase for $L_G=80nm$ because the channel is too thick (150nm) and because of a parasitic capacitance due to unwanted proximity between the gate head and the source contact after oxide polishing (see Fig.6). F_{MAX} higher than 200 GHz is reached for $2x35\mu m$ devices thanks to smaller R_G .

The continuous wave (CW) large signal performance of the transistors was measured using an on-wafer vectorial multi-harmonic Load-Pull (LP) setup. The fundamental frequency was set to 28GHz, with second harmonic tuning on both source and load. The source and load impedances were set for optimum PAE (Power Added Efficiency). The tuners were connected directly to the probes for improved impedance coverage (DELTA tuners from Focus Microwaves). The reference HEMT was measured at different bias points, with $PAE_{MAX}= 47.2\%$ and $P_{SAT}=2.93W/mm$ at $V_{DD}=10V$ (Fig.19). At $V_{DD}=20V$, the device shows a $PAE_{MAX}=41.1\%$ and $P_{SAT}=6.58W/mm$. A HEMT with $W_G=2x35\mu m$ is more efficient with $PAE_{MAX}=51.5\%$ at $V_{DD}=8V$ and 49.5% at $V_{DD}=10V$ (Fig.20). Table 2 summarizes LP results on various

device geometries. An estimation of the reference device temperature rise is obtained from measured DC power as a function of P_{IN} and a transistor thermal resistance, R_{TH} of 116 K/W, extracted by IR thermal imaging on the same transistor fabricated on a very similar epi stack [10]. The high thermal conductivity of the GaN:C back-barrier (compared to AlGaIn based), close to the heat source, allows the device temperature to remain below $135^\circ C$ ($30^\circ C$ chuck) at a P_{OUT} of 6.6 W/mm (Fig.21).

High power density has been reached in this work thanks to 1) high drain current available with AlN barrier 2) low substrate RF losses 3) low lag 4) delayed forward gate injection due to SiN gate insulator allowing large gate swing (Fig.10a) and 5) reasonable R_{TH} with GaN:C back-barrier. A benchmark of PAE versus $P_{OUT_{MAX}}$ is shown in Fig.22. This power performance is close to the best GaN/Si results at $V_{DS}=10V$ and shows that this technology can approach GaN/SiC power density performance around 30 GHz for PA applications at higher voltages. Fig.23 compares the F_{MAX} versus F_t of the reference device in this work with other GaN transistors with same or lower L_G . This work shows state of the art F_t and F_{MAX} for $L_G=150nm$ when compared to GaN/SiC devices with comparable L_G and competitive performance when compared to other GaN/Si devices with lower L_G .

III. CONCLUSION

CMOS compatible 200mm SiN/AlN/GaN MIS-HEMT on Silicon demonstration is reported. Low damage gate process and low temperature ohmic contacts integrated on high N_s/μ AlN based heterostructure with in-situ SiN gate dielectric leads to high current (1.8A/mm), high $G_{m_{MAX}} (>600mS/mm)$ and high CW $P_{OUT} (>6.5W/mm)$ at 28 GHz. This work brings GaN/Si HEMT closer to GaN/SiC performance at 28 GHz in terms of power density and highlights SiN/AlN/GaN on silicon MIS-HEMT as a potential candidate for high power Ka-band PAs. It is foreseen from those results that device performance can be further improved by reduction of R_c and optimization of channel thickness to reduce SCE for short gate lengths.

ACKNOWLEDGMENT

The authors would like to thank ST Microelectronics-Crolles and III-V Lab teams for fruitful discussions and financial support, Focus Microwave for LP measurements and IEMN for their contribution to IR thermography measurements. This work was supported by IPCEI European Project.

REFERENCES

- [1] K. Shinohara et al, IEEE TED, vol.60, no.10, p.2982, 2013; [2] T.E. Kazior et al, IMS, Tu4E-1, 2022; [3] B. Parvais et al IEDM p.155, 2020; [4] H.W. Then et al, IEEE microwave and wireless technology letters, p.1, may 2023; [5] H. Du et al., IEEE EDL, p. 1, 2023; [6] E. Kacou, EDICON 2019; [7] K. Arrouche, IMS 2020, Tu3H-2,p.285; [8] R. Elkashlan et al, IMS, Th2E-2, 2022; [9] H.W. Then et al, IEDM 2021 p.231; [10] A. Chanuel PhD thesis p.131; [11] R. Elkashlan et al, IMS, Tu1B-5, 2023 ; [12] E.M. Chumbes et al, IMS, Tu4E-3, 2022 ; [13] M. Mi et al., TED vol.64,n.12,p.4875, 2017 ; [14] K. Arrouche et al, Journal of the EDS, vol.7,p.1145,2019; [15] S. Piotrowicz et al, Eumic 2016,p.69; [16] Y. Cui et al, IMS,We1G-3, 2020; [17] D.F. Brown et al, IMS, Tu2B-4, 2023; [18] R.S. Howell et al, IMS 2023; [19] H.Xie et al, IEEE microwave and wireless components letters, vol. 31,no.2,feb 2021.

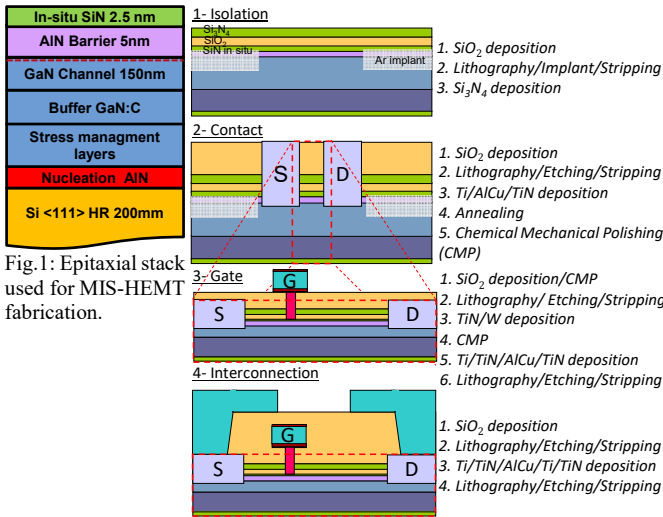


Fig.1: Epitaxial stack used for MIS-HEMT fabrication.

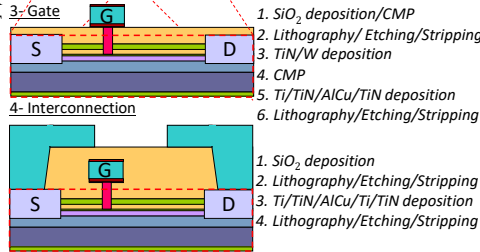


Fig.2: Process flow of the coplanar 2 finger devices.

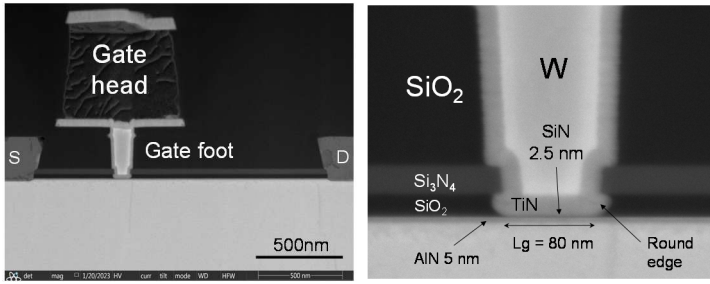


Fig.6: **Left:** STEM cross-section of the transistor showing asymmetry of L_{GS} and L_{GD} and large gate head section to achieve low R_G . Very good S/D edge definition is obtained with contact recessing, low temperature annealing and planarization. **Right:** STEM cross-section of a 80nm gate foot showing the conformal gate metal (TiN), the 2.5nm in-situ SiN gate dielectric, the 5nm AlN barrier and the rounded gate edge.

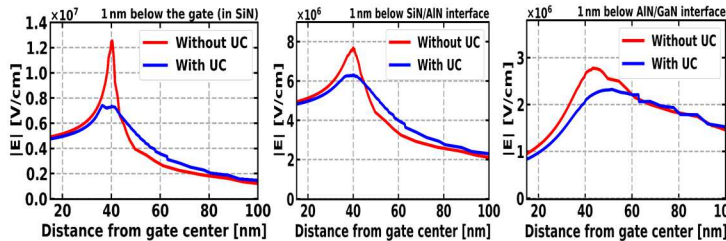


Fig.8: Simulated 1D Electric field magnitude ($|E|$) profiles for $V_{DS}=10V/V_{GS}=-5V$ at constant depth below the gate showing 42%/18%/18% reduction of $|E|$ in in-situ SiN, AlN barrier and GaN channel layers respectively, due to undercut.

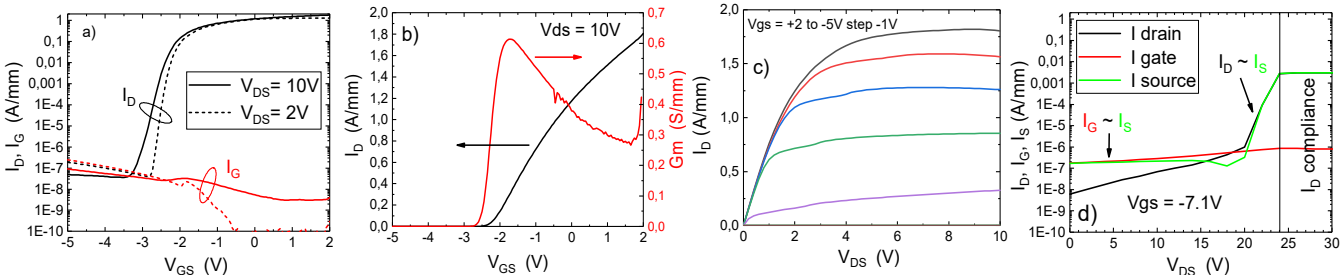


Fig.10: typical DC characteristics of $2 \times 50 \mu m$ HEMT ($L_G = 150 nm$). **a)** I_D and I_G (V_{GS}) at $V_{DS}=10V$ and $2V$ showing good pinch-off behavior, no forward gate injection at $V_{GS}=+2V$ and low gate leakage current thanks to in-situ SiN gate dielectric (3 orders of magnitudes lower than the corresponding Schottky gate leakage, not shown). **b)** I_D and G_m (V_{GS}) at $V_{DS}=10V$ showing a maximum drain current of 1.8 A/mm at $V_{GS}=+2V$ and a peak g_m of 610 mS/mm. **c)** I_D (V_{DS}, V_{GS}) **d)** I_D , I_G and I_S (V_{DS}) in off-state showing a low V_{DS} regime with low drain current and a source current driven by G-S leakage ($I_S \sim I_G$) and a high V_{DS} regime above 20V where the drain current is driven by a D-S leakage with negligible gate current. The non-destructive drain current compliance (3mA/mm) is reached at $V_{DS}=24V$. The two terminal G-D diode breakdown voltage with $L_G=150nm$ is $35 \pm 2.5V$ (not shown).

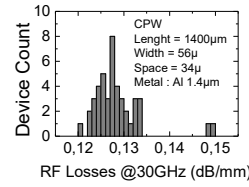


Fig.3: normalized RF losses distribution at 30 GHz.

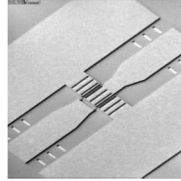


Fig.4: SEM top view of the coplanar $2 \times 50 \mu m$ transistor at Metal 1 level with GSG in/out.

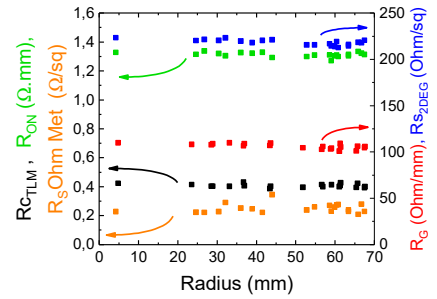


Fig.5: Uniformity of R_c , R_{ON} , R_{S2DEG} and R_G as a function of radial position on the wafer.

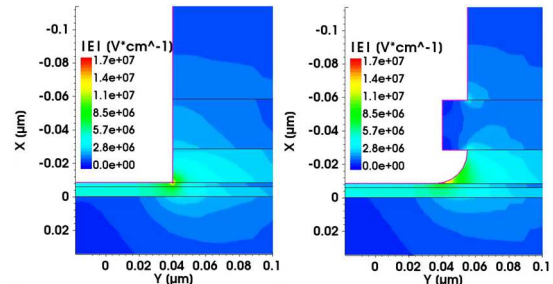


Fig.7: TCAD simulations of the Electric field magnitude ($|E|$) at the drain side of the gate foot on the reference transistor at $V_{GS}/V_{DS} = -5V/10V$, w/o UC (left) and with UC (right) in the oxide layer.

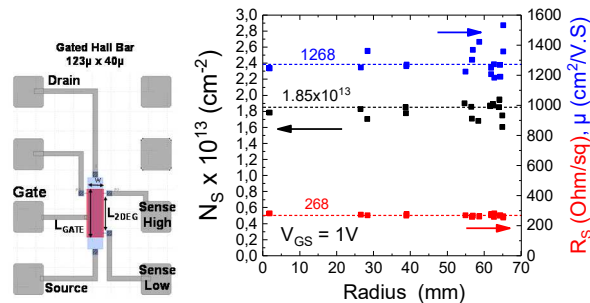


Fig.9: Extraction of low field channel parameters with a gated Hall bar structure (left). R_S is measured with 4 points probe technique. N_S is obtained by integration of $C(V_{GS})$ and $\mu = 1/(N_S \cdot q \cdot R_S)$ where q is the electronic charge. Uniformity across the wafer is shown in the right graph for $V_{GS} = +1V$ with median values of R_S , N_S and μ .

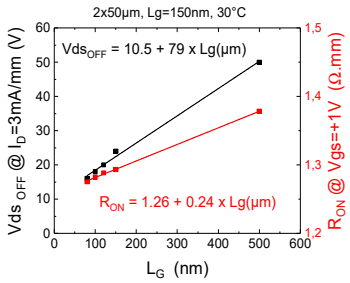


Fig.11: $V_{DS\ OFF}(L_G)$ at $V_{GS}=-7.1V$ and $I_D=3mA/mm$ (black). Degradation of $V_{DS\ OFF}$ with L_G is due to a short channel effect. $R_{ON}(L_G)$ (red) is dominated by access resistance, mainly R_c (~60%).

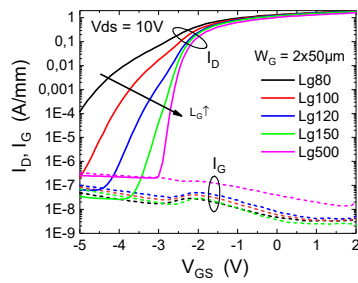


Fig.12: Impact of L_G on $I_D(V_{GS})$ (bold) and $I_G(V_{GS})$ (dot). Short L_G suffer from insufficient 2DEG confinement due to non-optimum channel thickness (150nm), which leads to V_P shift.

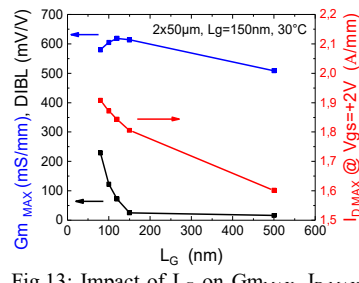


Fig.13: Impact of L_G on $G_{m\ MAX}$, $I_{D\ MAX}$ and DIBL. Although $I_{D\ MAX}$ increases for shorter L_G , V_P shift degrades G_M . DIBL is 25mV/V for $L_G=150nm$ but degrades strongly for smaller L_G .

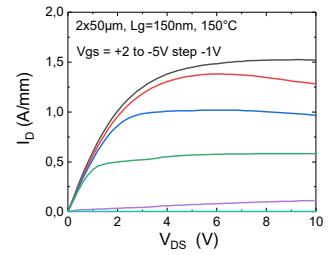


Fig.14: Reference HEMT $I_D(V_{DS})$ at 150°C. $I_{D\ MAX}$ reduction is mainly due to a decrease of the saturation velocity with temperature.

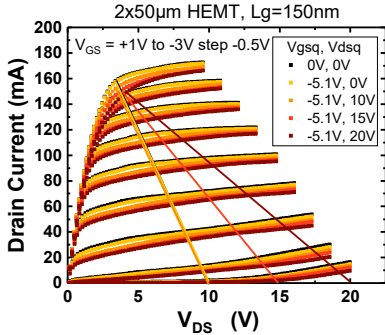


Fig.15: Pulsed-IV characteristics of a 2x50μm HEMT with $L_G=150nm$. Each point of the $I_D(V_{DS}, V_{GS})$ curves is pulsed from a given stress bias point (V_{gsq}, V_{dsq}). GL is negligible (light orange vs black curves) and DL is low up to 20V (dark red vs black curves). Straight lines are optimum load-lines for output power.

Die	GL (%)	DL10 (%)	DL15 (%)	DL20 (%)	$I_{D\ max}$ (A/mm)
0	0.4	4.0	7.9	10.2	1.69
1	0.4	3.6	6.9	9.6	1.73
2	0.5	3.3	6.6	10.5	1.84
3	1.4	1.8	4.8	8.0	1.81
Mean	0.67	3.17	6.55	9.57	1.76

Table 1: Pulsed-IV results on 4 dies across a wafer radius. Gate Lag (GL) is extracted from $V_{GS}/V_{DS} = V_{GS\ OFF}/0V$ and Drain Lags ($DL_{10,15}$ and 20) are extracted from $V_{GS}/V_{DS} = V_{GS\ OFF}/10, 15$ and 20V, respectively.

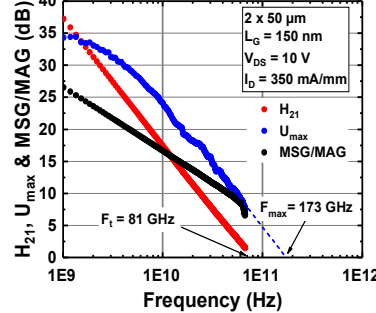


Fig.16: 2x50μm HEMT H_{21} , U_{max} and MSG/MAG versus frequency. Extrapolation gives $F_t/F_{MAX} = 81/173$ GHz.

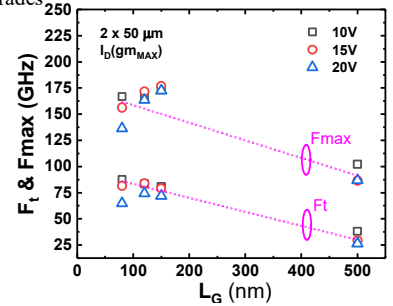


Fig.17: F_t and F_{MAX} vs L_G at $V_{DS} = 10, 15$ and 20V and I_D at $G_{m\ MAX}$.

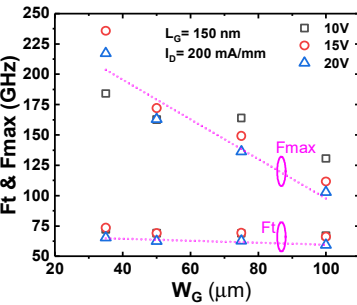


Fig.18: F_t and F_{MAX} vs gate Width (W_G) at $V_{DS} = 10, 15$ and 20V and $I_D=200mA/mm$. The reduction of R_G for smaller W_G leads to an increase of F_{MAX} above 200 GHz.

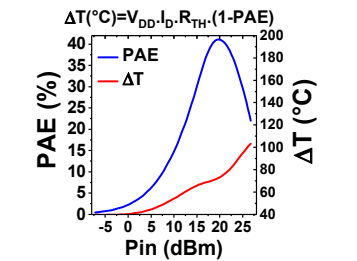


Fig.21: Calculation of device temperature rise as a function of P_{IN} and PAE with $R_{TH}=116$ K/W.

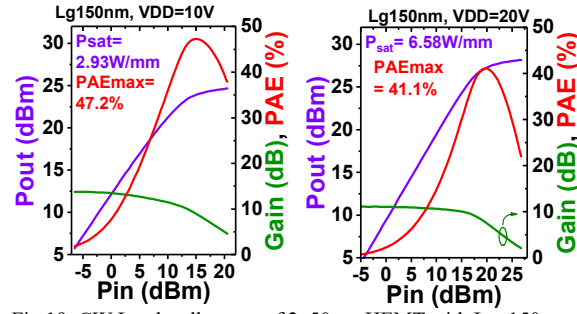


Fig.19: CW Load-pull sweep of 2x50μm HEMT with $L_G=150nm$ at 28 GHz. We obtain state of the art $P_{OUT,MAX}$ of 2.9 W/mm at $V_{DD}=10V$ and record 6.6W/mm at $V_{DD}=20V$ for a CMOS compatible 200mm SiN/AIN/GaN/Si MIS-HEMT.

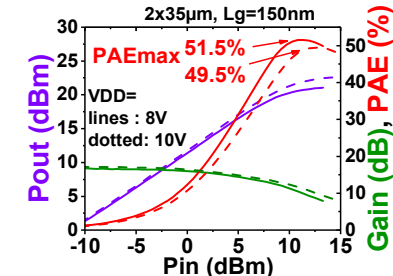


Fig.20: CW Load-pull sweep of 2x35μm HEMT with $L_G=150nm$ at 28 GHz. The device reached 51% PAE at $V_{DD}=8V$ and 17dB linear power gain.

L_G (nm)	W_g (μ)	V_{DS} (V)	PAE_{MAX} (%)	$P_{OUT}@PAE_{MAX}$ (W/mm)	P_{SAT} (W/mm)
150	2x50	10	47.2	2.17	2.93
		15	45.33	3.25	3.61
		20	41.1	4.94	6.58
150	2x35	8	51.5	1.68	1.83
		10	49.5	2.39	2.62
		8	46.6	1.98	-
80	2x50	10	41	2.52	3

Table 2: PAE , P_{OUT} at max PAE and P_{SAT} for different device geometries and bias voltages.

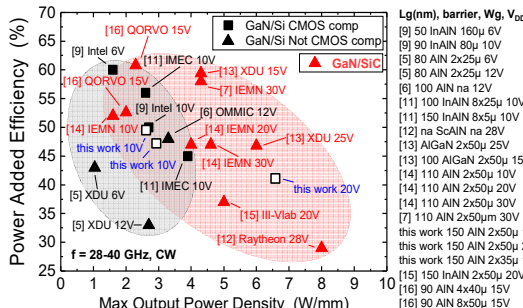


Fig.22: CW PAE vs max P_{OUT} benchmark at 28-40 GHz. GaN/Si (black) and GaN/SiC (red). CMOS compatible (square) and non-compatible (triangles). This work (blue) shows state of the art at 10V and high power density at 20V, similar to GaN/SiC.

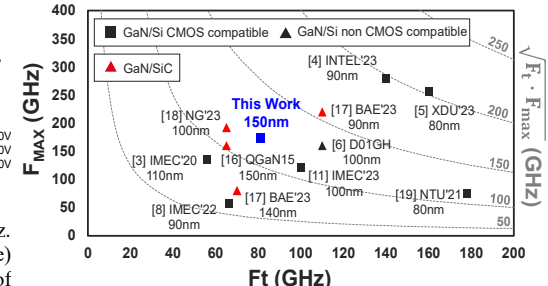


Fig.23: Comparison of F_{MAX} vs F_t for GaN/Si (black) and GaN/SiC (red) devices for L_G between 80nm and 150nm. This work (blue) shows state of the art F_t and F_{MAX} for $L_G=150nm$.